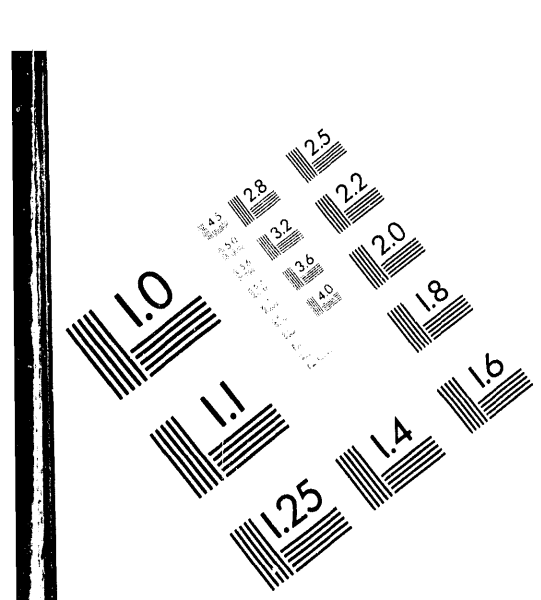

Association for Information and Image Management

1100 Wayne Avenue, Suite 1100
Silver Spring, Maryland 20910

301/587-8202

Centimeter

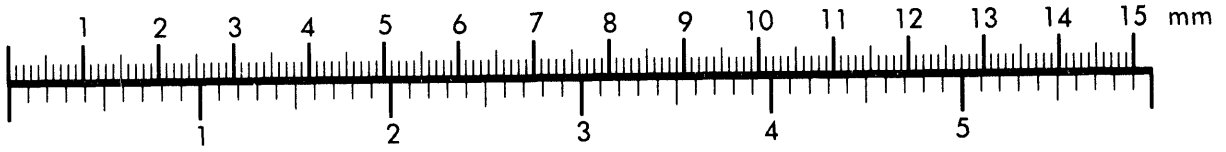

Inches

MANUFACTURED TO AIIM STANDARDS
BY APPLIED IMAGE, INC.

1 of 1

Ionization Balance and Gain Calculations for Neon-like Selenium X-Ray Laser Plasmas*

A. L. Osterheld, R.S. Walling, B.K.F. Young, W.H. Goldstein, G. Shimkaveg,
B.J.MacGowan, L.Da Silva, R. London, D. Matthews, R.E. Stewart
Lawrence Livermore National Laboratory, L-59
P.O. Box 808, Livermore, CA 94550

ABSTRACT

We have developed compact collisional-radiative models to describe the ionization balance and excitation mechanisms in neon-like selenium x-ray laser plasmas. These models can be used for calculations of the ionization dynamics, detailed emission spectra, and gain coefficients. Careful attention has been paid to indirect processes such as dielectronic recombination, excitation–autoionization, and resonant excitation. We discuss the importance of different atomic processes and model approximations in the ionization balance and gain calculations. These results will be compared to experimental measurements and to previous calculations.

INTRODUCTION

The use of highly charged ions in plasmas to produce lasing action at short wavelengths has been studied by many groups.[1-3] The most successful results have been obtained with collisional excitation lasing schemes[4-5] in neon-like ions[6-8]. The first unambiguous demonstration of soft x-ray lasing observed amplification of 3p-3s transitions in neon-like selenium[9]. These experiments used "exploding foil" laser produced plasmas as the laser medium[10], as schematically shown in figure 1. Later, similar results were obtained in experiments utilizing simpler, solid targets.[11]

The design of x-ray lasers involves large scale simulations of the heating and expansion of the plasma, the changing degree of ionization and excitation of the plasma, and the propagation of the x-ray laser beam through the inhomogeneous amplifying medium. These simulations are typically decoupled into three parts.[12,13] A simple atomic model is used in conjunction with a hydrodynamics code to predict the interaction of the heating laser with the target, and the expansion and evolution of conditions in different regions of the plasma. This prediction for the plasma conditions is used to drive a time dependent calculation of the atomic kinetics. Accurate predictions of the gain

coefficients require a detailed model of the atomic processes of the ions in the plasma. The propagation of the x-ray laser beam through the refractive plasma medium is typically treated by ray-tracing techniques.

The remainder of this paper describes the atomic physics codes and the methods and approximations we use to model atomic processes in x-ray laser design calculations. The influences of different atomic processes are displayed by steady state calculations of ionization balance and gain coefficients for collisionally pumped neonlike selenium x-ray lasers. The atomic model is coupled to a hydrodynamic calculation to simulate the transient gain produced in an exploding foil x-ray laser. Propagation of the x-ray laser beam is discussed in the context of a simple refraction model, a more complete treatment using ray tracing techniques[14] is left for future work.

COLLISIONAL–RADIATIVE MODEL METHODOLOGY

A collisional-radiative atomic model is a collection of energy levels and their associated transition rates and is used to construct the collisional-radiative rate matrix.

$$\frac{dn_j}{dt} = \sum_i n_i R_{i\to j} - n_j \sum_i R_{j\to i} \qquad (1)$$

Here, nj is the population of level j, and $Ri\to j$ is the rate coefficient for transitions between level i and level j. These equations describe the various excitation, ionization, and recombination processes which populate and depopulate the energy levels. This atomic data is used by a plasma simulation code to calculate plasma conditions, and the degree of ionization and excitation of the plasma. X-ray laser design calculations place two different demands on the degree of precision in the atomic models. Calculations of plasma conditions and ionization dynamics require an approximate description of atomic processes for a large number of atomic levels, while calculations of gains require a very detailed description of the atomic processes for a subset of the energy levels. Thus, our

collisional-radiative models consist of detailed atomic data embedded in an average-level model.

The detailed atomic data come from the Hebrew University-Lawrence Livermore Atomic Code package (HULLAC) originally developed at Hebrew University. This code is used to calculate wave functions, energy levels, autoionization rates, and all important radiative transition rates from the relativistic, multi-configuration parametric potential model.[15-17] Relativistic, distorted wave electron excitation cross-sections are calculated for all transitions.[18] The cross-section calculations use a powerful angular factorization and an empirically motivated interpolation scheme for calculating radial integrals. This code package uniquely combines accuracy and highly efficient computational techniques and enables practical calculations of even very complex atomic systems.

The detailed levels are surrounded by an average level model. The energy levels, radiative and collisional transitions, and photoionizations are constructed from subshell energies and transition rates obtained from a Hartree-Slater code of J. Scofield.[19] As discussed further below, rates for some of the indirect processes are obtained from configuration average autoionization rates of Chen.[20] Collisional ionizations and three-body recombinations are based on subshell rates from the Refs. 21–23.

In addition to singly excited states, a many electron ion has multiply excited states which have energies above the ionization potential of the ion. The energy level diagram in figure 2 schematically displays the important processes involving these multiply excited levels. The enormous number of such levels for a complex ion present significant difficulties for collisional radiative calculations. In calculations of intermediate density plasmas, we approximate the effect of these levels by additional indirect contributions to excitation, ionization, and recombination processes. These represent the composite processes which couple singly excited levels via transitions

through intermediate autoionizing levels. Such composite processes include resonant excitation, excitation-autoionization, and dielectronic recombination. Typically, a variety of approximations are used in calculations of the indirect processes. For ionization sequences near a closed shell, we use large scale calculations of energies and radiative and autoionization decay rates[17] of the doubly excited states to compute rate coefficients for the indirect processes. For some of the complex, open shell ionization sequences, we use configuration average calculations for these composite processes[20].

NEON-LIKE SELENIUM X-RAY LASER PLASMAS

A highly simplified level scheme for neon-like selenium is shown in figure 3. The main predicted lasing transitions are a J=0–1 transition at 182 Å, and two J=2–1 transitions at 206 Å and 209 Å. The J=0–1 transition is excited mainly by a monopole electron impact excitation rate, while the J=2–1 transitions are fed by many channels of excitation, recombination, and ionization followed by radiative and collisional cascades. The inversions are produced because the upper states are metastable, while the lower states have large $\Delta n=1$ allowed transitions to the ground state. While predicted to have the largest gain, the J=0–1 transition was originally not observed. Over time, the magnitude of this discrepancy was reduced, though not eliminated, as the theoretical gains dropped, and the line was experimentally observed. The most recently published comparison[24] is summarized in table 1. A further puzzle was the absence of predicted lasing on fluorine-like 3p-3s transitions.[25] The fluorine-like transition with the highest predicted gain is analogous to the neon-like J=0–1 transition. In addition to calculations performed at Livermore, recent publications have presented steady state ionization balance calculations for selenium at conditions relevant to x-ray laser experiments,[26,27] as well as steady state calculations of gain coefficients for the important lasing

transitions.[27] Both of these publication differ significantly from results published by Livermore scientists.

Since the large lasing transitions occur in specific charge states, it is important to understand the ionization dynamics of the highly charged ions in x-ray laser plasmas. As noted above, the presence of multiply-excited states gives rise to additional ionization and recombination processes. The importance of these indirect processes has long been recognized. However, owing to the difficulty of treating these processes in a non-LTE, dense plasma, they have frequently been inconsistently treated or partially ignored. The importance of the indirect ionization processes is illustrated in figure 4. This shows the temperature dependence of various contributions to the ionization of the 3s ground level in sodium-like selenium. The indirect ionizations proceeding through states of the form $1s^2 2s^2 2p^5 3l3l'$ and $1s^2 2s^1 2p^6 3l3l'$ are larger than the total direct ionization rate. More highly excited autoionizing states increase the ionization rate further. The indirect contributions dominate the ionization rate.

The effect of the indirect ionization and recombination processes on the ionization balance of selenium is shown in figure 5. The steady state abundance of neon-like ions is shown (for $n_{ion} = 1\times10^{19}$ cm^{-3}, corresponding to $n_e \approx 2.5\times10^{19}$ cm^{-3}) as a function of electron temperature for several calculations. The curve labeled a) ignores all of the indirect processes, while curves b) and c) include just the dielectronic recombination and both the dielectronic recombination and excitation-autoionization, respectively. The indirect ionization and recombination processes significantly affect the ionization dynamics, and must be treated carefully and consistently. This was also pointed out in Ref. 26, although their results are different quantitatively (compare Fig. 5 to Fig. 3 of Ref. 26).

Because of the large number of ionic states of a complex ion, it is tempting to calculate the ionization dynamics with an average level model. This procedure works

well for LTE (local thermodynamic equilibrium) or very low density plasmas, but is not suited to plasmas at intermediate density. When a large fraction of the ions are near an ion stage with a closed shell ground state (such as neon-like), there are many metastable excited states. A significant fraction of the ions can be in excited states, which are much more easily ionized either directly, or by step-wise ionization. An average level model treats metastable levels and resonantly decaying levels together, and typically underestimates the excited state populations, and thus, the collisional-radiative ionization rate. Figure 6 illustrates the large effect the treatment of the excited states has on the ionization dynamics. The calculations of Ref. 26 used a configuration average atomic model and yielded results similar to the configuration average results (dashed curves) shown in Fig. 6. These results also disagree dramatically with the ionization balance calculations in Ref. 27, the reason is unclear at present. At the intermediate density used in the calculations in Fig. 6, the present calculations agree well with results from the "standard" selenium atomic model used in recent Livermore calculations.[25] (This density is typical of the most important gain regions of neon-like selenium lasers). There are differences between the calculations at both lower and higher densities; the ultimate effects of these differences in x-ray laser simulations is under study.

As noted above, there are several discrepancies between measured and predicted gain coefficients in the neon-like selenium experiments. Figure 7 compares steady-state gain calculations from the atomic model developed in the present work to results from the atomic model used in earlier Livermore calculations.[25] Several qualitative effects are evident. The gain for the 182 Å J=0–1 transition has dropped relative to the J=2–1 transitions. This caused by changes in the ionization balance calculations, a decrease in the monopole excitation rate and increases in the n=3–3 collisional mixing rates. In addition, the gain for the "missing" fluorine-like analog to the 182 Å transition has dropped by a factor of two. This is almost entirely owing to a decrease in the monopole

excitation rate of the upper state. The gains of the three neon-like transitions shown in Fig. 7 are substantially different than results reported in Ref. 27. These difference become even more prominent at higher density. A more complete discussion of the mechanisms for producing gain in neon-like selenium ions will be given in a future publication.

Experimental values measured for gain coefficients result from a complicated interplay of the plasma hydrodynamics, the time dependent ionization balance, the excitation mechanisms, and laser propagation. Results are shown here for a simulation of an exploding selenium x-ray laser. The target was 725Å of selenium on a 1000Å CH backing. The target was illuminated from two sides by 500 psec gaussian beams of 0.53μm light with intensities of 3.5×10^{13} W/cm^2 per beam. The width of the line-focus was 120 μm. These parameters are similar to the original selenium experiments.[9] The heating and expansion of the plasma was calculated with the LASNEX[28] hydrodynamic code. A one-dimensional slice (at the center of the line focus, along the direction of the heating laser) was post-processed with the XRASER[29] collisional radiative modeling code. The spatial dependence of gain profiles for the three main transitions are shown in Figs. 8a and 8b for 200 psec before the peak and at the peak of the drive laser, respectively. The J=0–1 transition has highest gain at the early time, but has dropped significantly lower than the two J=2–1 transitions by the peak of the pulse. As has been pointed out earlier,[10] the problem of refraction caused by the large electron density gradient is greatest early in time. Calculations which treat the refraction using a geometric ray tracing post-processor are underway. However, a qualitative picture can be obtained from a simple model of the refraction. The rate of deflection of the x-ray laser beam passing through region with an electron density gradient can be estimated from[1]

$$\frac{d\theta}{dz} = \frac{r_0}{2\pi}\lambda^2\frac{dN_e}{dr}. \qquad (2)$$

Here, r_0 is the classical electron radius, λ is the x-ray laser wavelength, and dN_e/dr is the transverse electron density gradient. Figures 8c and 8d display the results of this simple model for the angular deflection. The x-ray laser amplifiers are typically a few centimeters long, and light which is refracted by more than 15 mrad, or so, may be ignored. As this model shows, the highest gain regions at early times—when the J=0–1 transition has highest gain—contributes little to the x-ray laser output. A rough idea of the evolution of the important gain regions may be obtained by following the gains in the region behind the large density gradient in figure 8. The time histories of the gain coefficients in this region are shown in figure 9. The gain of the J=0–1 transition peaks at early time, and quickly falls below the main J=2–1 lines. A more complete treatment of the outputs of the x-ray laser transitions, including the temporal and spatial variation of the gain coefficients, trapping effects, and a ray-tracing calculation of the x-ray laser propagation will be reported in future work.

CONCLUSIONS

We have described collisional-radiative models developed for complex non-LTE neon-like selenium x-ray laser plasmas. These new calculations have revealed partial explanations for old puzzles about the magnitudes of gain coefficients in selenium x-ray laser experiments. In addition, these calculations differ substantially from other calculations recently reported. While space precludes a description here, an experimental program to test these x-ray laser calculations—both the collisional-radiative models and the hydrodynamic simulations—is underway. These efforts include measurements of fundamental atomic rates and cross-sections, line formations processes in intermediate density plasmas, and temperature and density measurements in x-ray laser plasmas. A report on some of these experiments may be found in these proceedings.[30]

ACKNOWLEDGMENTS

*Work performed under the auspices of the U.S. Dept. of Energy by the Lawrence Livermore National Laboratory under Contract No. W-7405-Eng-48.

REFERENCES

1. R.C. Elton, *X-ray Lasers*, (Academic, New York, 1990), and references therein.
2. *X-ray Lasers 1992, Proceedings of the 3rd Inernational Colloquium on X-ray Lasers,* IOP Conf. Series, editor E. Fill (IOP, Bristol, England, 1992).
3. C.H. Skinner, *Phys. Fluids B* **3**, 2320, (1991).
4. R.C. Elton, *Appl. Optics* **14**, 97 (1975).
5. L.J. Palumbo and R.C. Elton, *J. Opt. Soc. Am.* **67**, 480, (1977).
6. A.N. Zherikin, K.N. Koshelev, V.S. Letokhov, *Sov. J. Quant. Electron.* **6**, 82, (1976).
7. A.V. Vinogradov, I.I. Sobel'man, and E.A. Yukov, *Sov. J. Quant. Electron.* **7**, 32, (1977).
8. A.V. Vinogradov and V.N. Shlyaptsev, *Sov. J. Quant. Electron.* **10**, 754, (1980), and **13**, 303 and 1511 (1983).
9. D.L. Matthews, P.L. Hagelstein, M.D. Rosen, M.J. Eckart, N.M. Ceglio, A.U. Hazi, H. Medecki, B.J. MacGowan, J.E. Trebes, B.L. Whitten, E.M. Campbell, C.W. Hatcher, A.M. Hawryluk, R.L. Kauffman, L.D. Pleasance, G. Rambach, J.H. Scofield, G. Stone, T.A. Weaver, *Phys. Rev. Lett.* **54**, 110, (1985).
10. M.D. Rosen, P.L. Hagelstein, D.L. Matthews, E.M. Campbell, A.U. Hazi, B.L. Whitten, B. MacGowan, R.E. Turner, R.W. Lee, *Phys. Rev. Lett.* **54**, 106, (1985).
11. T.N. Lee, E.A. MacLean, and R.C. Elton, *Phys. Rev Lett.* **39**, 1185, (1987).
12. R.A. London, M.D. Rosen, M.S. Maxon, D.C. Eder, P.L Hagelstein, *J. Phys B* **22**, 3363, (1989).
13. M.D. Rosen et al 1988 *AIP Conference Proceedings 168 – Atomic Processes in Plasmas, Santa Fe*
14. R.F. Ratowsky, R.S. Craxton, M.D. Feit, R.A. London, R.S. Walling, G>M. Shimkaveg, A.L. Osterheld, M.R. Carter, *Proceedings of the 3rd Inernational Colloquium on X-ray Lasers, AIP Conference Proceedings 125,* 315, (1992).
15. M. Klapisch,*Comput. Phys. Commun.* **2** 239, (1971).
16. M. Klapisch, J.L. Schwob,B.S. Fraenkel J. Oreg, *J . Opt. Soc. Am.* **61** 148 (1977).
17. J. Oreg, W.H. Goldstein, M. Klapisch, A. Bar-Shalom, *Phys. Rev. A* **44**, 1750, (1991).
18. A. Bar-Shalom, M. Klapisch, J. Oreg, *Phys. Rev. A* **38**, 1773, (1988).
19. E.B. Saloman, J.H. Hubble, J.H Scofield, *Atomic Data and Nuclear Tables* **38**, 1, (1988).
20. M.H. Chen, *Phys. Rev. A* **40**, 2758, (1989).
21. D.H. Sampson, L.B. Golden, D.L. Moores, *Ap. J.* **170**, 169, (1971).
22. D.L. Moores, L.B. Golden, D.H. Sampson, *J. Phys. B* **13**, 385, (1980).
23. L.B. Golden, R.E.H. Clark, S.J. Goett, D.H. Sampson, *Ap. J. Suppl.* **45**, 603, (1981).
24. B.J. MacGowan, L.B. Da Silva, D.J. Fields, C.J. Keane, J.A. Koch, R.A. London, D.L. Matthews, S. Maxon, S. Mrowka, A.L. Osterheld, J.H. Scofield, G. Shimkaveg, J.E. Trebes, R.S. Walling, *Phys. Fluids B* **4**, 2326, (1992).
25. P.L. Hagelstein, *Phys. Rev. A* **36**, 924, (1986).
26. J. Abdallah, R.E.H. Clark, J.M. Peek, *Phys. Rev. A* **45**, 3980, (1992).
27. A. Dasgupta, K.G. Whitney, M. Blaha, M. Buie, *Phys. Rev. A* **46**, 5973, (1992).
28. G.B. Zimmerman and W.L. Kruer, *Com. Plasma Phys. and Cont. Fusion* **2**, 85, (1975).
29. P.L. Hagelstein, Lawrence Livermore National Laboratory Report No. *UCRL-53100* (1992).

30. B.K.F. Young, A.L. Osterheld, G.M. Shimkaveg, R.L. Shepherd, R.S. Walling, W.H. Goldstein, R.E. Stewart, these proceedings, (1993).

TABLE CAPTIONS

Table 1 The most recently published theoretical and experimental gain values are summarized (from reference 24).

FIGURE CAPTIONS

Figure 1 An exploding foil x-ray laser plasma is produced by focusing optical laser pulses on each side of a thin foil. A hot, roughly cylindrical, intermediate density plasma is produced in the blowoff region, where the inversion is created. The conditions and laser parameters shown are typical for selenium x-ray laser experiments.

Figure 2 A many electron ion has many multiply-excited states that are energetically above the ionization potential of the ion. The diagram schematically shows the important types of levels involved in the multi-step dielectronic recombination, resonant excitation, and excitation-autoionization processes.

Figure 3 The important levels in the collisionally excited neon-like selenium x-ray lasing scheme are shown (not to scale). The 182 Å J=0–1 inversion is produced by a strong monopole excitation, while the J=2–1 lines are produced by excitations and recombinations followed by cascades. The lower levels decay by fast resonant transitions to the ground state.

Figure 4 Rate coefficients for the important ionization processes of the sodium-like Se ground state are shown. Here, valence refers to ionization of the 3s electron, inner shell includes all 2s and 2p ionizations, and excitation-autoionization refers to a collisional excitation from n=2 to n=3, followed by autoionization.

Figure 5 The indirect ionization and recombination processes dramatically affect the ionization balance selenium ions. The steady state ionization fraction of neon-like selenium as a function of temperature for an ion density 1×10^{19} cm^{-3}. Three calculations are shown: a) with no indirect processes, b) with the dielectronic recombinations, and c) with both dielectronic recombination and excitation-autoionization processes.

Figure 6 The degree of ionization is affected by the treatment of excited states. Two calculations of the steady state ionization fractions of neon-like, sodium-like and fluorine-like selenium ions are shown for an ion density 1×10^{19} cm^{-3}. The bold curves are from a calculation which treats important metastable levels as detailed, fine structure levels. The plain curves were calculated using the same atomic rates, except the metastable levels were treated as configuration average levels.

Figure 7 Steady state gain coefficients for neon-like selenium at Nion = 4×10^{18} cm^{-3} for the 206 Å (dashed) and 209 Å (dot-dashed) J=2–1 transitions, the 182 Å J=0–1 (solid) transition, and the strongest fluorine-like analog (dotted) to the 182 Å line.

Figure 8 Spatial profiles for the main gain transitions of neon-like selenium from a hydrodynamic simulation (see text) are shown for snapshots a) 200 psec before the peak of the drive laser b) at the peak of the pulse. Plots c) and d) display estimates of the angular refraction of the propagating x-ray laser beam obtained from a simple refraction model (see text).

Figure 9 Temporal profiles of the main gain transitions of neon-like selenium are shown for the region of plasma behind the large density gradient, i.e. for the zone at r=20μm in fig. 8a.

wavelength (Å)	α_{theor} (cm^{-1})	α_{exp} (cm^{-1})
206.4	5.8	4.1
209.8	6.3	3.9
182.4	6.0	2.5

Table 1

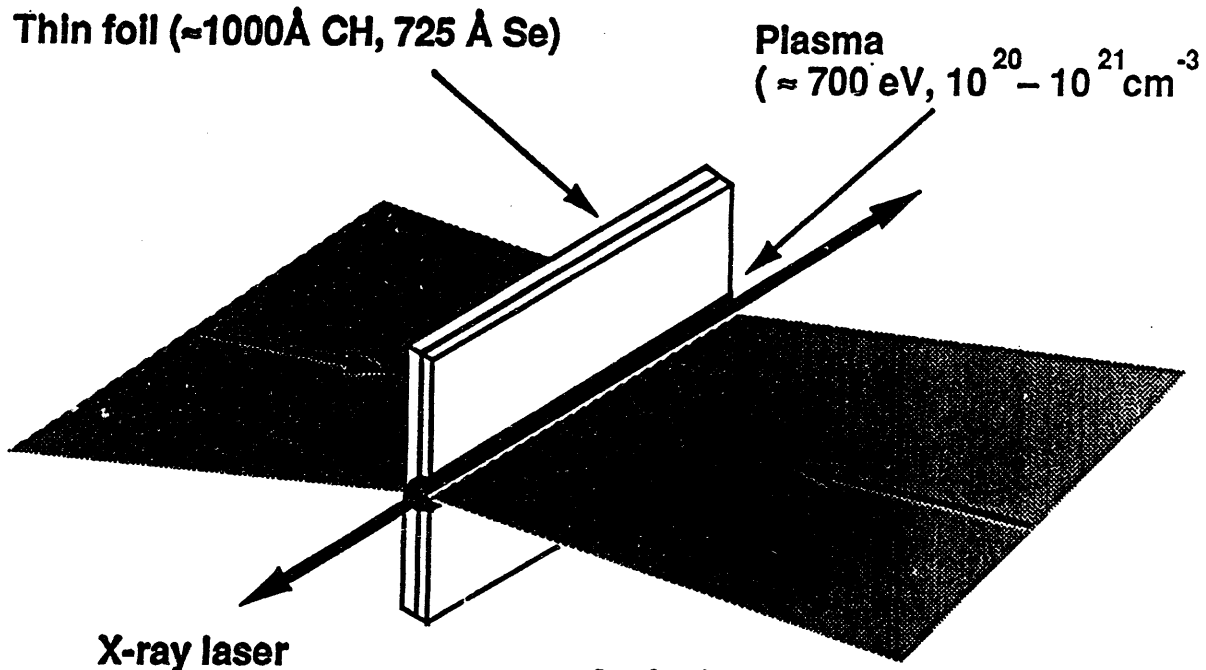
Thin foil (≈1000Å CH, 725 Å Se)
Plasma
(≈ 700 eV, 10^{20} – 10^{21} cm^{-3})
X-ray laser
beam
Optical pump laser
focus ≈ 120μm
λ = 0.53 μm
500 psec gaussian pulse
I ≈ 3.5x10^{13} W/cm^2 per beam

Figure 1

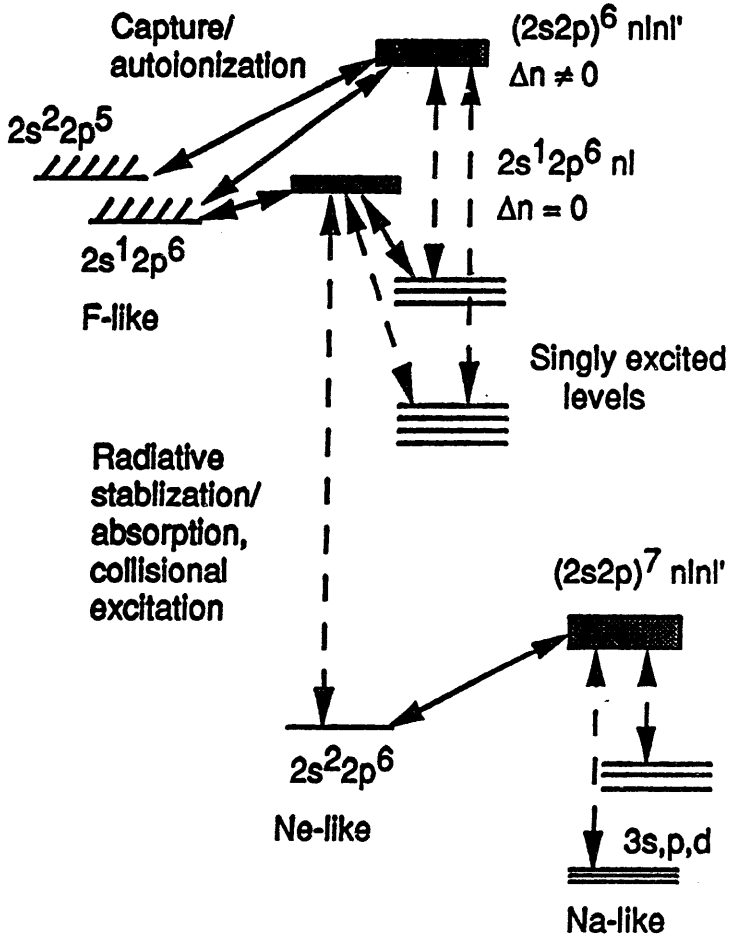
Capture/
autoionization
$(2s2p)^6$ nlnl'
$\Delta n \neq 0$
$2s^2 2p^5$
$2s^1 2p^6$ nl
$\Delta n = 0$
$2s^1 2p^6$
F-like
Singly excited
levels
Radiative
stablization/
absorption,
collisional
excitation
$(2s2p)^7$ nlnl'
$2s^2 2p^6$
Ne-like
3s,p,d
Na-like

Figure 2

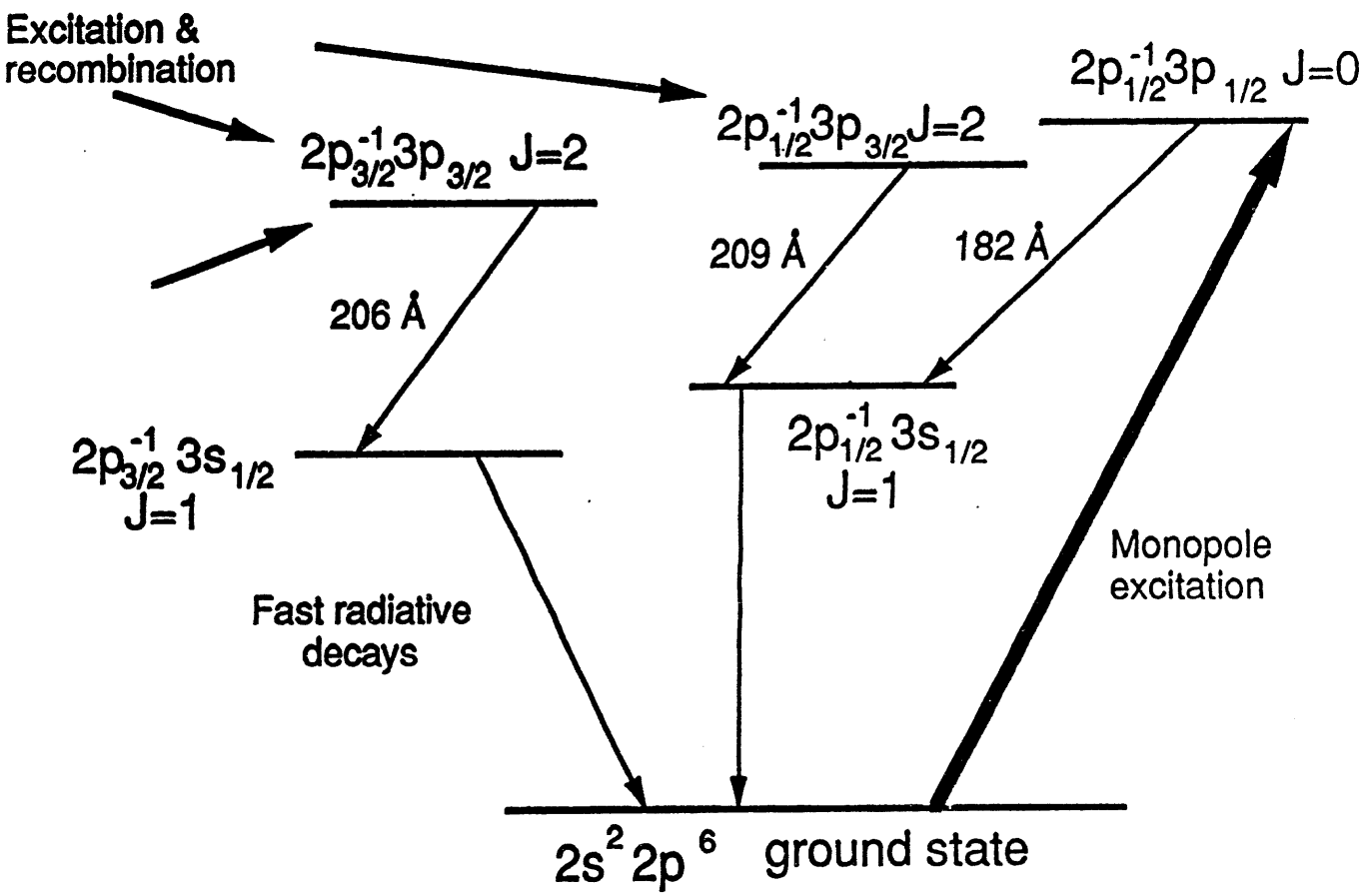
Excitation &
recombination
$2p_{3/2}^{-1}3p_{3/2}$ J=2
$2p_{1/2}^{-1}3p_{3/2}$J=2
$2p_{1/2}^{-1}3p_{1/2}$ J=0
206 Å
209 Å
182 Å
$2p_{3/2}^{-1}3s_{1/2}$
J=1
$2p_{1/2}^{-1}3s_{1/2}$
J=1
Fast radiative
decays
Monopole
excitation
$2s^2 2p^6$ ground state

Figure 3

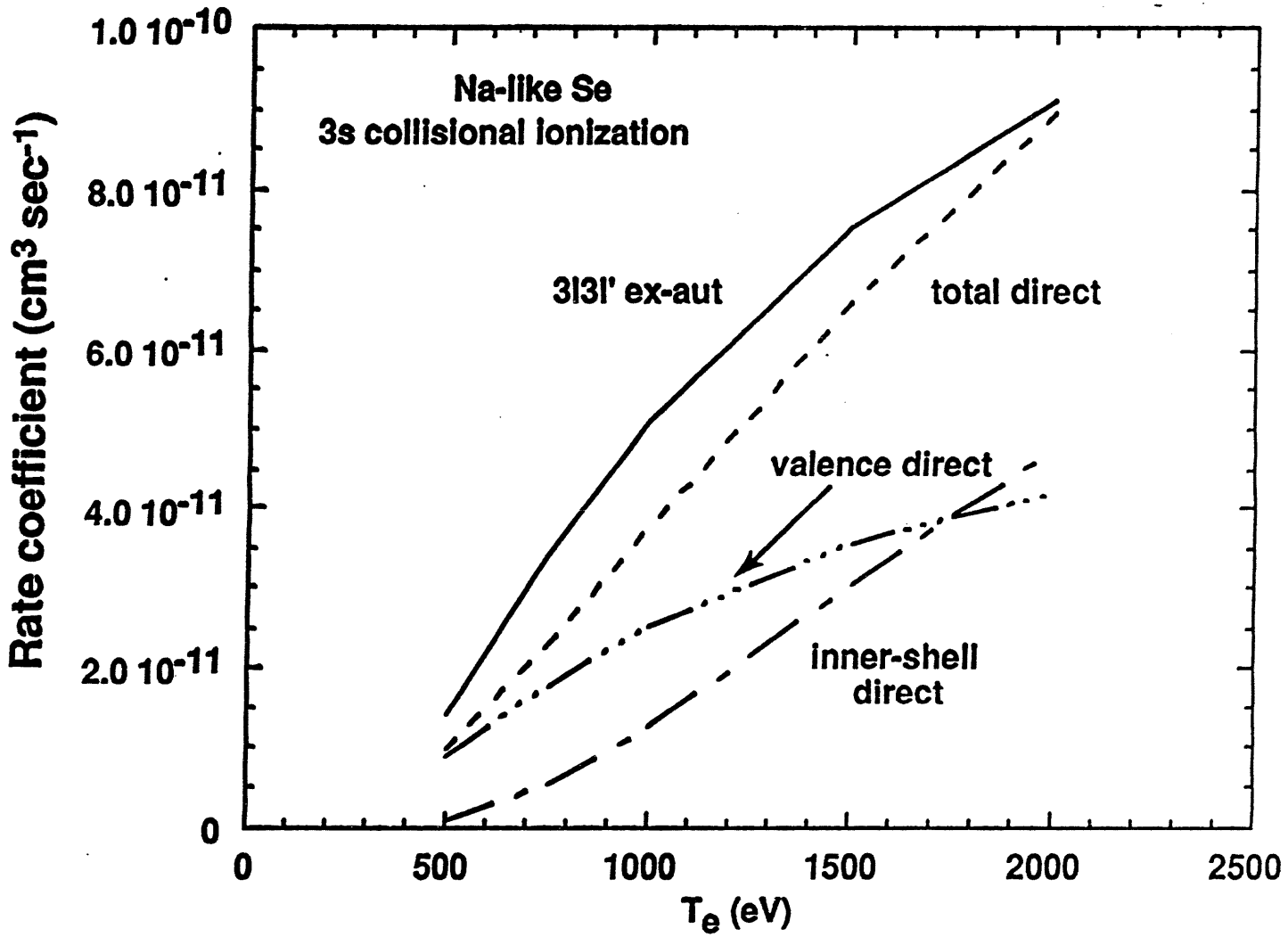
Na-like Se
3s collisional ionization
3l3l' ex-aut
total direct
valence direct
inner-shell
direct
Rate coefficient (cm3 sec-1)
1.0 10-10
8.0 10-11
6.0 10-11
4.0 10-11
2.0 10-11
0
0
500
1000
1500
2000
2500
Te (eV)

Figure 4

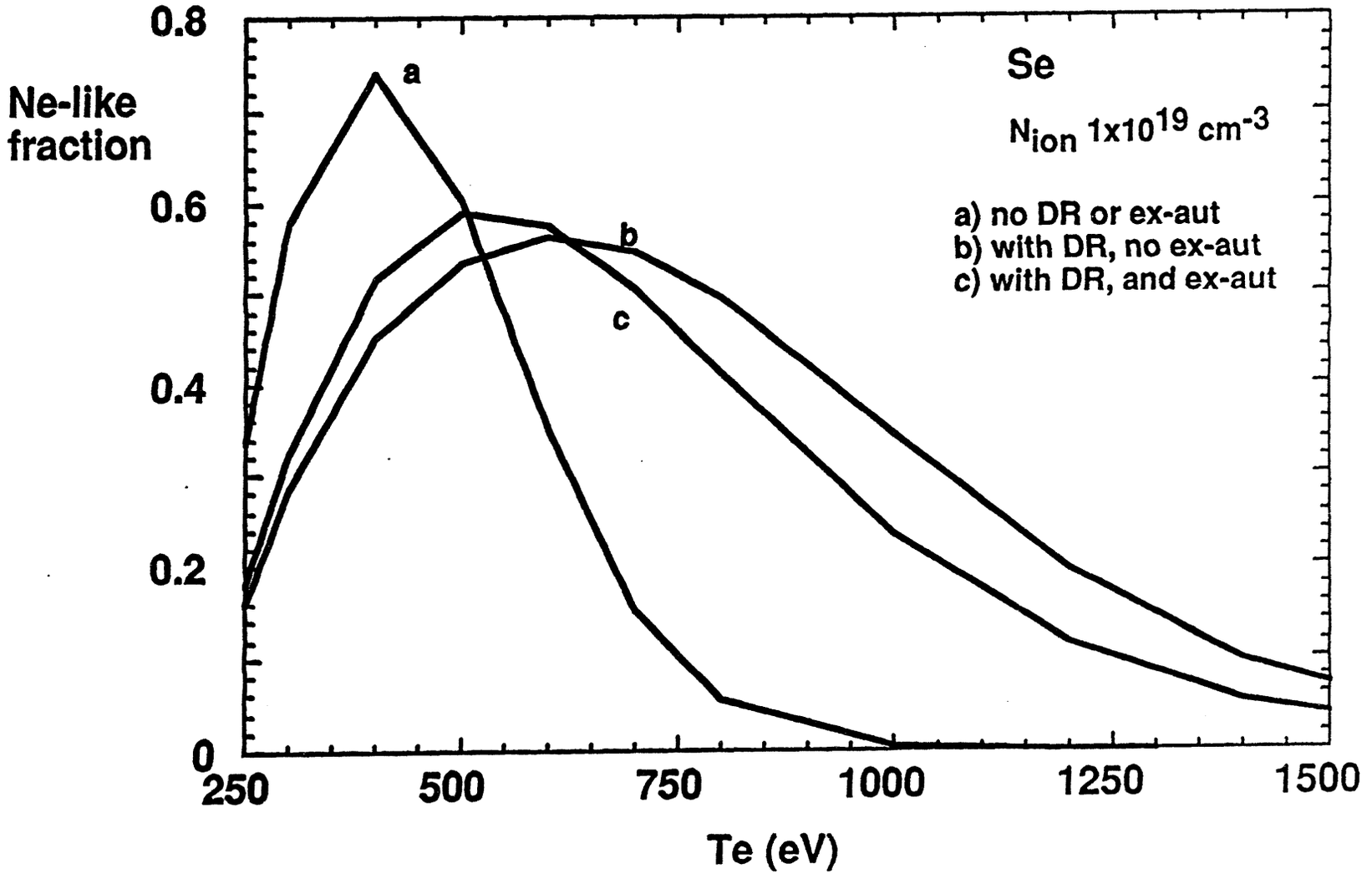
Ne-like fraction
0.8
0.6
0.4
0.2
0
250
500
750
1000
1250
1500
Te (eV)
Se
N_{ion} 1x10^{19} cm^{-3}
a) no DR or ex-aut
b) with DR, no ex-aut
c) with DR, and ex-aut
a
b
c

Figure 5

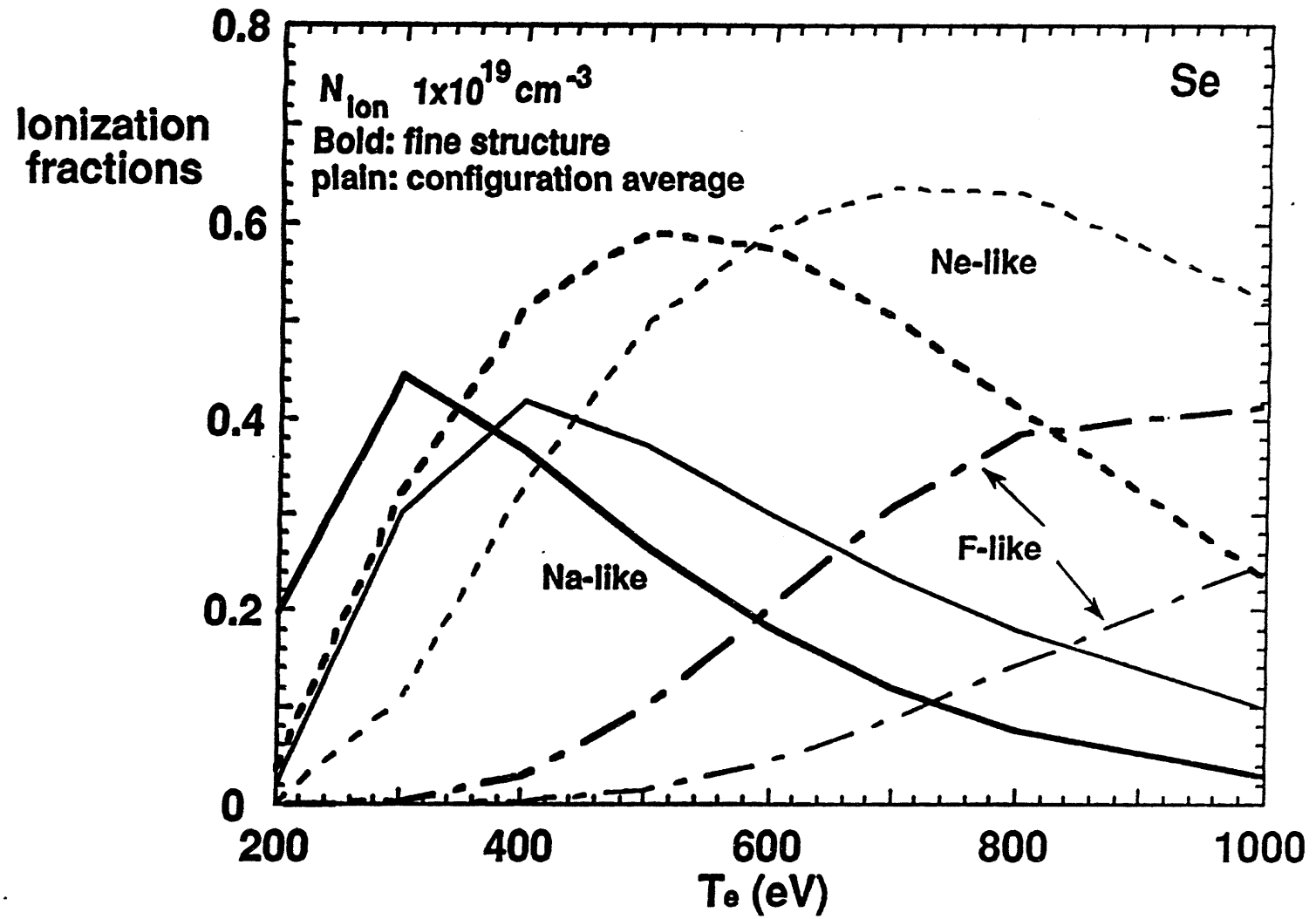
Ionization fractions
0.8
0.6
0.4
0.2
0
N_{Ion} 1x10^{19} cm^{-3}
Bold: fine structure
plain: configuration average
Se
Ne-like
F-like
Na-like
200
400
600
800
1000
Te (eV)

Figure 6

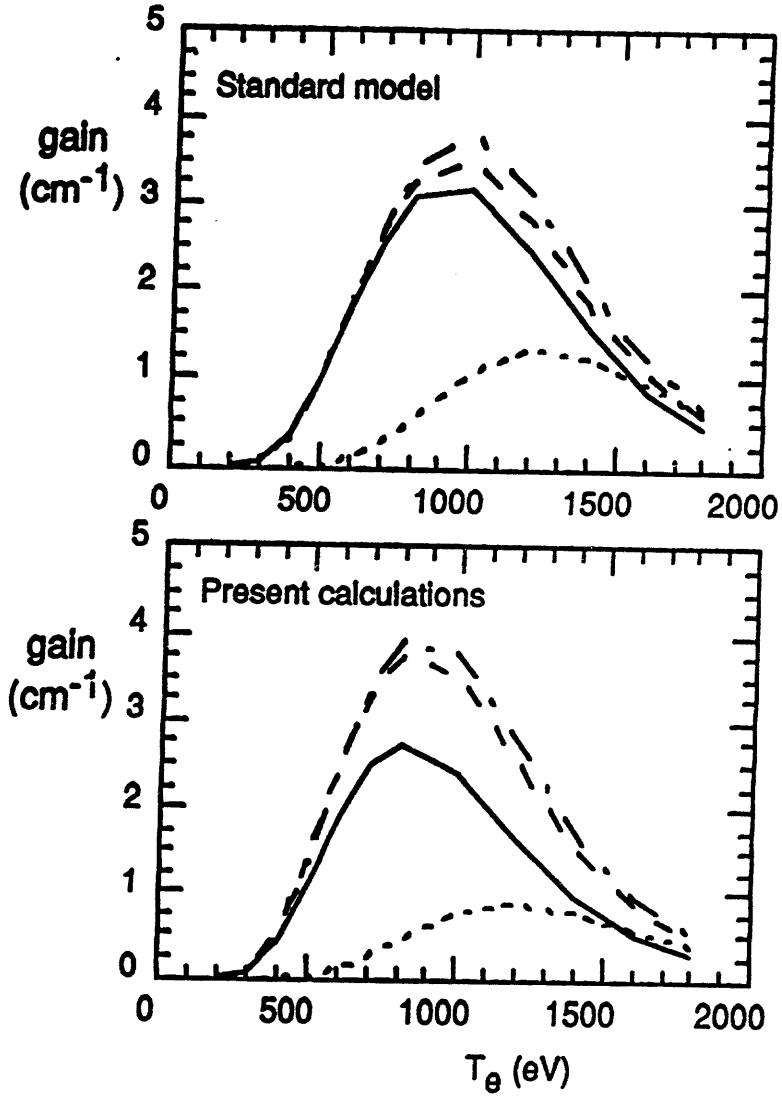
Standard model
gain
(cm^{-1})
0
1
2
3
4
5
0
500
1000
1500
2000
Present calculations
gain
(cm^{-1})
T_e (eV)

Figure 7

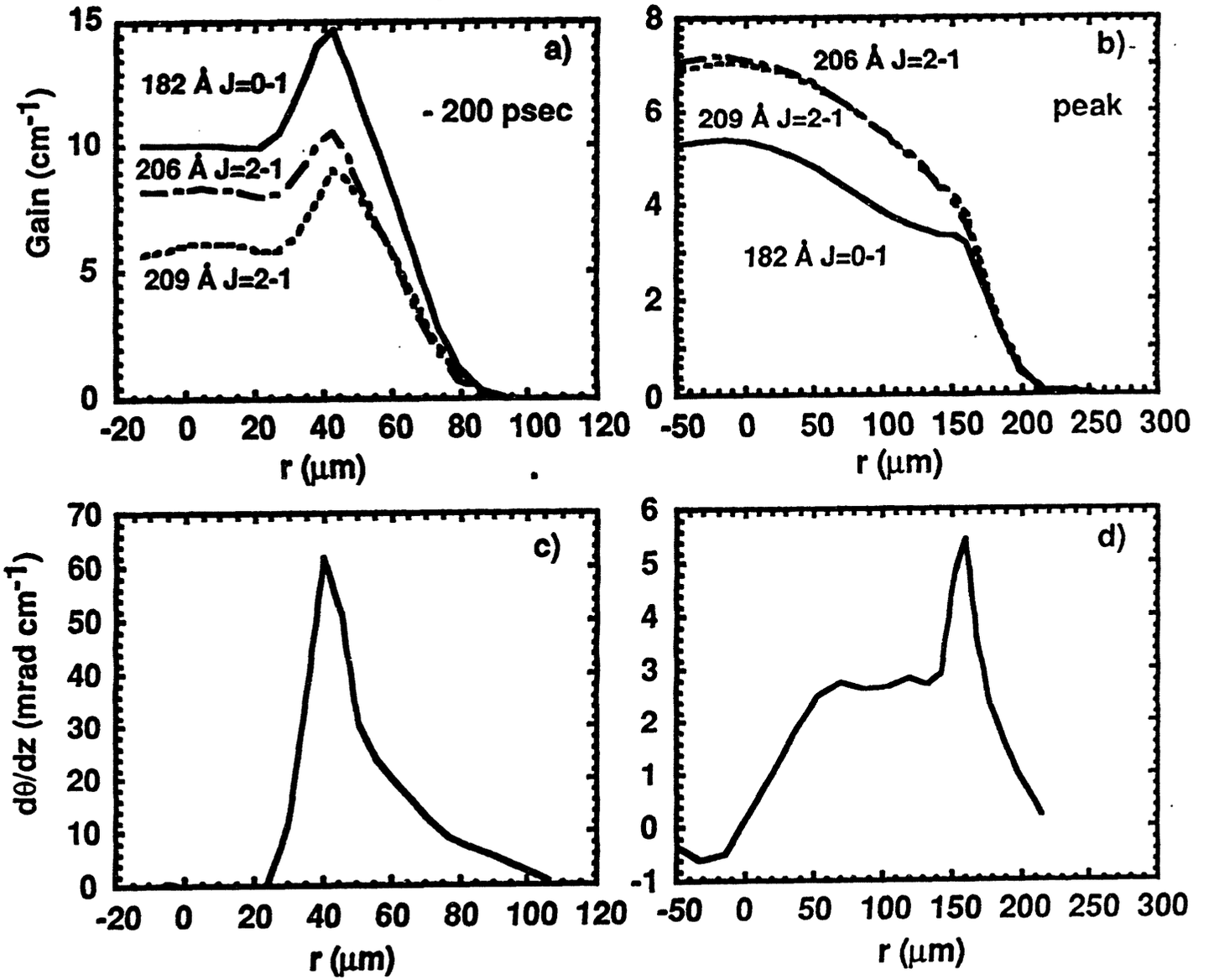
a)
182 Å J=0-1
206 Å J=2-1
209 Å J=2-1
- 200 psec
Gain (cm^{-1})
r (μm)
b)
206 Å J=2-1
209 Å J=2-1
182 Å J=0-1
peak
r (μm)
c)
dθ/dz (mrad cm^{-1})
r (μm)
d)
r (μm)

Figure 8

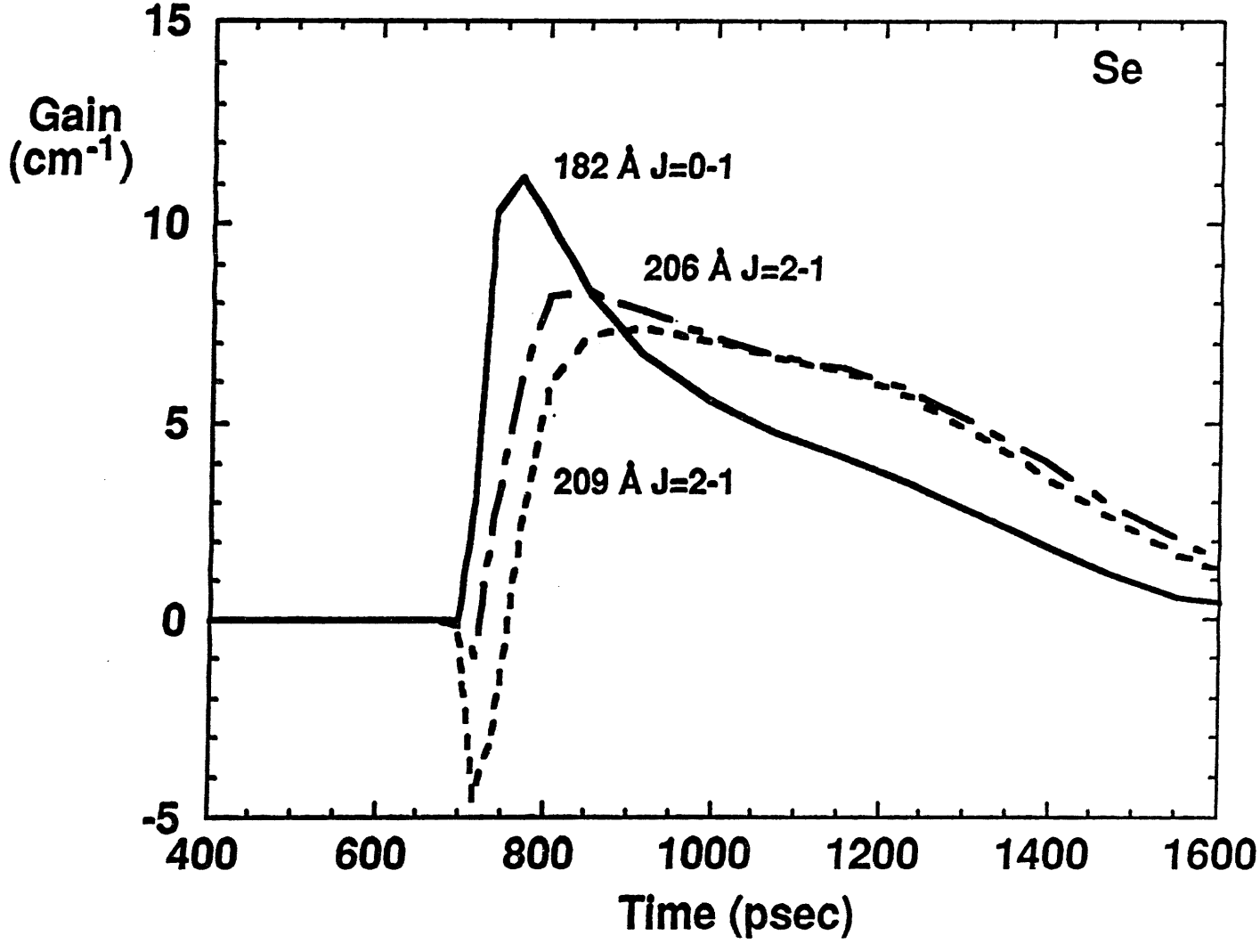
Se
Gain
(cm-1)
182 Å J=0-1
206 Å J=2-1
209 Å J=2-1
15
10
5
0
-5
400
600
800
1000
1200
1400
1600
Time (psec)

Figure 9

DATE
FILMED
6/29/94
END